Pyrolyzed 3D Metallic Nanolattices via Two-Photon Lithography

Sammi Cheung, David Vacek, Swaroop Kommera, and Tony Ricco

ENGR 241, Spring 2023

1. Introduction

1.1 Motivation

3D nano-architected materials promise superior control over structural properties for a vast array of applications, such as strong and lightweight porous materials for bone implants, efficient electronic cooling channels, or tunable photonic crystals [1, 2, 3]. Recent advancements in 3D printing technology such as two-photon lithography have enabled fast fabrication and customization of structures at the nanoscale, while maintaining accuracy and resolution [4, 5]. Two-photon lithography, combined with pyrolysis-induced shrinkage of polymer structures, has demonstrated hierarchically ordered structures at the smallest feature size currently possible in additive manufacturing [6, 7, 8].

However, more work is still necessary to explore the limits of feature sizes in two-photon lithography, and to develop a universal set of procedures that can achieve specified designs. At the pyrolysis step, more optimization of experimental parameters is needed to achieve desired shrinkage rates and explore the possible distortions that may result. Further, the metallization of these resulting nanolattices poses a new set of challenges. Electroplating optimization is needed to achieve uniform, tunable thicknesses of metal on the sample surface.

We demonstrated nano-architected glassy carbon structures fabricated via two-photon lithography and pyrolysis. The three types of structures, along with metal electroplating to be improved in future work, enable design versatility with possible applications in mechanics, optics, and electronics.

1.2 Benefits for the Stanford Nanofabrication Facility (SNF)

We developed procedures to fabricate nano-architected structures with high customizability to user needs, high shrinkage rates and robust adhesion for nanoscale carbon structures, and tunable electroplating procedures for metal plating.

Our project comprises a generalizable set of methods which can help SNF users from many different fields. Demonstrations of diverse nanostructure samples with superior optical, electronic, and mechanical properties are relevant to a variety of applications. The use of standard materials such as Nanoscribe default photoresists and substrates make the process repeatable without requiring users to purchase excessive materials. Additionally, previous work has not focused on the effect of furnace conditions on shrinkage rate, nor the techniques required to conformally metallize pyrolyzed structures and etch out the interior.

Thus, the project has three main goals:

1. Develop a Standard Operating Procedure (SOP) specifically geared towards writing structures in the Nanoscribe for further pyrolysis, using the dip-in laser lithography mode with the standard IP-Dip photoresist to make the process widely generalizable for other SNF users. We developed guidelines for laser power and scanning speed settings to achieve desired feature sizes.
2. Develop an SOP for pyrolysis of polymeric microstructures, with guidance on how to tune the shrinkage rate and purity of carbon with differing furnace operating parameters.
3. Develop an SOP for electroplating of pyrolyzed microstructures, with guidance on how to uniformly coat all surfaces and how to etch out carbon to create consistent feature sizes.

2. Methods

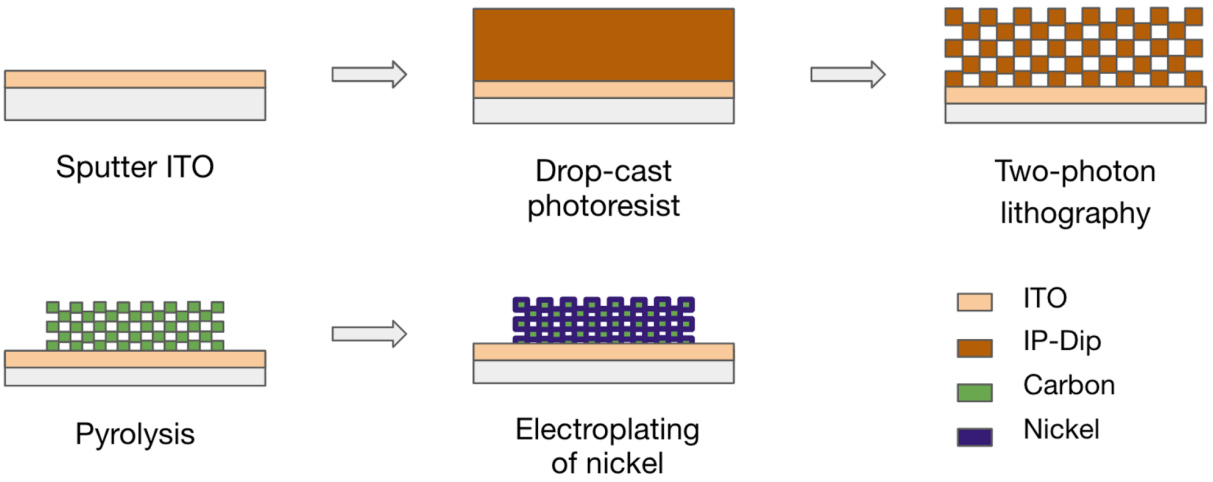

Fig. 1. Summary of fabrication process, which involves (1) sputtering 150 nm of ITO on fused silica substrate; (2) dropcasting IP-Dip photoresist on substrate; (3) exposure/development of test structures in the Nanoscribe via dip-in laser lithography; (4) pyrolysis of polymer test structures in furnace with Ar flow; and (5) electroless plating of nickel onto the structure surface.

2.1 Test Structures

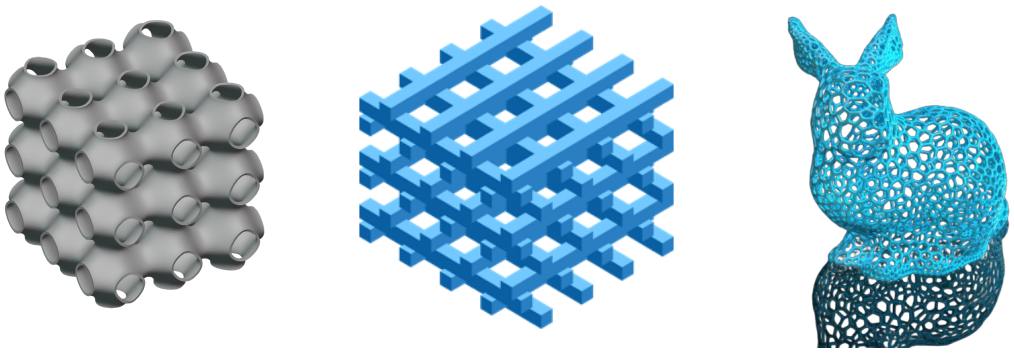

Fig. 2. Test structures, including a Schwarz Primitive TPMS lattice (left) for mechanical and thermal applications, a woodpile photonic crystal for optical applications (middle), and a lattice frame rabbit to demonstrate structure customizability (right).

We fabricated three test structures to demonstrate the universality of our methods. The first test structure, a Schwarz Primitive TPMS lattice, demonstrates superior mechanical and thermal performance for strong but lightweight material applications. The Schwarz Primitive lattice exhibits a wall thickness of 2 μm and a unit

cell edge length of 15 μm, for an overall edge length of 60 μm in a 16 unit cell cube. The second test structure, a woodpile photonic crystal, contains periodic high and low refractive indices to affect electromagnetic wave propagation for optical applications. The woodpile structure exhibits a strut thickness of 2 μm and an overall edge length of 60 μm. The third test structure, a lattice frame rabbit model, demonstrates the customizability of our methods to any arbitrary structure. The rabbit model reveals the complexity of possible structures, as well as any feature distortions that may result.

2.2 Lesker Sputter Deposition

Each of our original materials considered had their individual issues: standard Nanoscribe DiLL fused Silica was not conductive for electroplating, and Nanoscribe ITO coated glass had a melting point significantly lower than the temperatures required for Pyrolysis. The aim was to deposit a conductive surface layer ITO on Nanoscribe DiLL Fused Silica substrate that is heat resistant for the purposes of Pyrolysis and conductive for the purposes of electroplating. Replicating Nanoscribe documentation, we wanted a deposition layer of approximately 150nm thick. Since this layer was not part of our final structure, precise manufacture was not important.

We quantified the ITO thickness and resistivity. The profilometry graph produced by the Alphastep shows an approximate 1500A step (150nm) as seen in Figure 3 below.

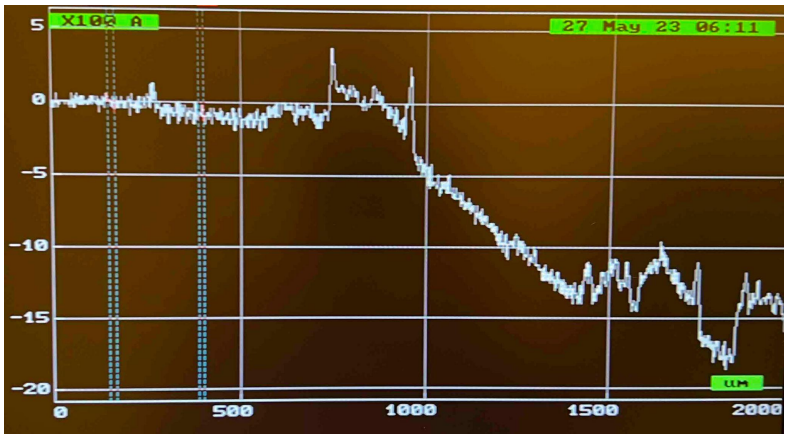

Fig. 3. Profilometry graph of the ITO surface using the Alphastep.

When measuring the resistivity, we obtained an average of approximately ~$5x10^{0}$ Ω cm. After pyrolysis, the resistivity lowered to approximately ~$7x10^{-2}$ Ω cm.

Hence, the final resistivity of the ITO surface was very similar and slightly larger than the resistivity of pyrolyzed carbon at ~$1.6x10^{-2}$ Ω cm. By matching these

resistivities, we optimize that our samples are conductive for Nickel electroplating and that Nickel is being similarly deposited on the sample and ITO surface; we are controlling the current density throughout the sample.

2.3 Nanoscribe Two-Photon Lithography

We fabricated the test structures via two-photon lithography in the Nanoscribe Photonics Professional GT, with dip-in laser lithography (DiLL) mode. The Nanoscribe proprietary negative photoresist, IP-Dip (refractive index around 1.57), was used along with the standard fused silica substrate. At the highest resolution with the 63x objective lens, the Nanoscribe can achieve a lateral feature size of 200 nm and a lateral resolution of 500 nm [9]. We operated the Nanoscribe in piezo scanning mode to achieve higher resolution [9]. The printed structures were then developed in SU-8 developer for 30 minutes, followed by a UV cure at 40°C for 30 minutes to increase the crosslinking within the polymer.

Our main focus during the Nanoscribe printing stage was to fine tune printing parameters such as layer height, laser power, and scanning speed to optimize the resulting structure fidelity. We printed a dose matrix of varying laser powers and scanning speeds to determine the minimum possible resolution. Decreased laser power can achieve smaller voxel sizes and lessen the risk of bubbling, but a laser power that is too low will not polymerize the photoresist.

We printed at a laser speed of 10000 um/s, with a solid laser power of 60% to increase the cross-linking within the IP-Dip polymer and prevent warping during pyrolysis. We increased the base slice count to span the entire pad below the structure, and used a laser power of 40% to reduce bubbling. The solid base is more likely to experience bubbling from the high exposure density and the higher effective dose at the interface due to the higher reflectivity of ITO on the surface.

We used an interface position of 4.0 um to increase the adhesion to the substrate. We also added a mesh block between the substrate and the test structure to reduce the strain mismatch and thus reduce the distortion of the bottom few layers of the test structure once shrinkage occurs [2].

2.4 Tube Furnace Pyrolysis

We achieved a 60% linear shrinkage rate of pyrolyzed structures, measured as the shrinkage rate of the side length of the lattice. We used a Thermo Fisher Scientific tube furnace to pyrolyze the IP-Dip lattices, at 900℃ for 60 minutes with an Ar gas flow at 3 L/min. We used a ramp rate of 4℃/min.

In order to avoid warping of the pyrolyzed samples, we used a supporting mesh structure below the lattices themselves to decouple the strain in the structure from the surface of the substrate. We also used a high laser power and a post-development UV cure to increase the polymer crosslinking.

In order to avoid delamination of the pyrolyzed samples, we printed a solid pad between the supporting mesh structure and the substrate to increase the adhesion to the surface. We also deposited HDMS with the yes oven and assigned a 4 μm interface position to the printing process to increase adhesion.

2.5 Electroplating

Pyrolyzed samples are conductive but extremely delicate. By plating structures with metal such as Nickel, we increase the mechanical strength of the structures and maintain, if not improve, its conductive properties as well.

For Nickel Electroplating, we used a commercial Nickel Sulfamate solution to electroplate, with a zinc sheet as the anode (opposing electrode) and a copper wire as the cathode connected to our substrate via conductive silver epoxy and copper tape (working electrode). To note, only our sample was submerged in the solution; the copper/silver additions allowed ohmic contact between the alligator clips and the sample.

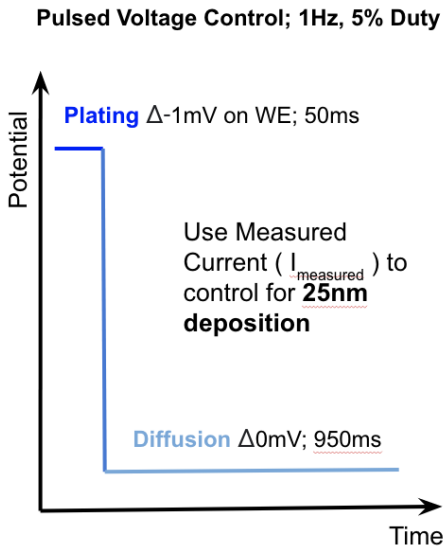

Fig. 4. One wavelength of the Pulsed Potential Control regime used for electroplating Nickel on pyrolyzed structures, using the BioLogic machine.

We used the BioLogic machine to precisely regulate the electroplating process via a pulse controlled potential regime. Since the microlattices have significant surface

area to volume ratio, this pulsed potential-control regime overcame the diffusion-limit plating process so that we can achieve plating uniformity on our structures. We found best results with a 1Hz, 5% duty cycle, with a very small overpotential via a controlled potential difference of -1 mV on the working electrode vs. the reference opposing electrode, as shown in Figure 4.

Additionally to ensure even plating on every surface of these microstructures, we evacuated trapped microbubbles within the surface by degassing the sample and solution in a vacuum chamber bell for no less than five minutes. While we believed that agitation of the samples would further promote convection through the lattice and lower the impact of diffusion-limits, our delicate structures would fall off their substrates when the solution was magnetically stirred or in an ultrasonic bath. We do not recommend agitation for this reason, and encourage a lower duty cycle or frequency of the electroplating regime.

For the structures selected, we aimed for a Nickel thickness of around 25 nm and achieved a nickel growth rate of 0.584 nm/(s A mm^2). Since plating thickness correlates with current, we integrated the measured current during plating to determine the necessary time for plating duration.

Regardless of the challenges, we were able to obtain nickel plating on the pyrolyzed resist structures. Since the ITO surface and structures were so similar in resistivity, any observable silver with the naked eye on the substrate could visually confirm the progression of plating on the pyrolyzed structures as well.

3. Results

3.1 Morphology Characterization

The FEI Nova NanoSEM 450 Scanning Electron Microscope (SEM) hosted in the Stanford Nano Shared Facilities (SNSF) was used to characterize the structure morphology. The SEM images clearly show the shrinkage rate of different parts of the test samples, to reveal any potential distortion in the structure.

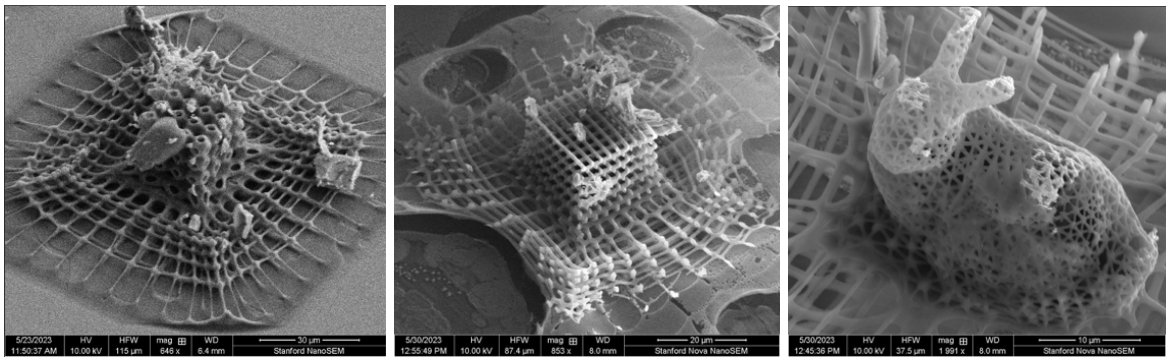

Fig. 5. SEM images of the three test samples, using the NovaSEM.

Furthermore, the NovaSEM was also used to characterize the extent of nickel electroplating. Our image shows 3 different structures; first, the ITO surface in the lower left, then the base layer of pyrolyzed structure, as well as the first layer of the sacrificial structure that mechanically disconnects our intended structure from the static substrate surface. The SEM image clearly shows Nickel grains electroplated on the ITO surface as well as on the base layer of the pyrolyzed structure. We can confirm nickel is electroplating on the pyrolyzed structure and not overflowing onto the pyrolyzed surface from the ITO surface because there are distinguishable islands of nickel grain electroplated on the first layer of the sacrificial structure.

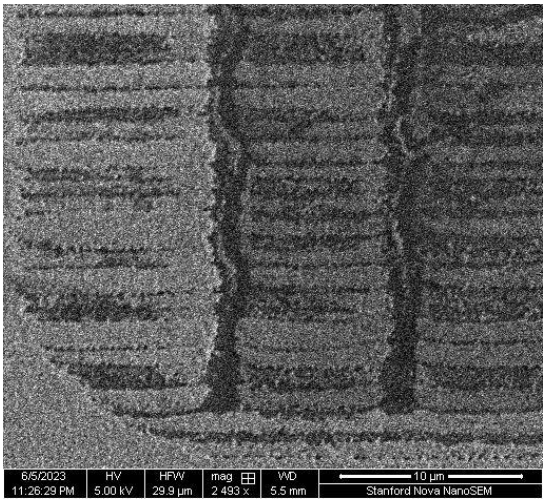

Fig. 6. SEM images of deposited nickel via electroplating on pyrolyzed structure, using the NovaSEM. There are clear islands of Nickel plating on the pyrolyzed resist that demonstrate Nickel plating on our structures.

In the future, We plan to improve structural integrity and adhesion during lithography and pyrolysis and refine the electroplating process to ensure a uniform metal coating over the sample. Additionally, we will fabricate smaller lattices to explore the resolution limit of two-photon lithography, as well as plasma etch the interior carbon to reveal hollow metal lattices.

4. Applications

The current project pushes the development of metamaterials, which are engineered materials with unusual, unique properties and advanced functionalities that are a direct consequence of their microarchitecture. While these structures have well documented applications in photonics and electromagnetism, research is demonstrating strong potential in acoustic, mechanics, biomaterials, and thermal engineering [11]. Here are only a couple examples of applications:

4.1 Electrical

The modern development of stacked 3D chips, especially in the neuromorphic industry, continues to pose questions about packaging that provides adequate structural integrity in lightweight form and strong thermal heat dissipation performance. Metallic Nanolattices increase the surface area providing better thermal cooling performance to intrinsically mechanically strong and thermally conductive materials.

4.2 Optical

Metallic lattices in different patterning and orientations create possibilities for applications in photonics. In particular, the precise manufacture of logpile nano structures manifests in a photonic bandgap where in a range of photonic energies which are forbidden to exist in this structure. These structures are known as photonic crystals and act as photonic analogs to semiconductors [10]. Photonic crystals are integrated into commercial, military, and molecular spectroscopy practices benefitting from photonic crystals' functionality in processing and emission of signal transmission.

4.3 Medical

Surgeons extensively use metal implants for invasive surgeries including joint replacements, pace-maker implants, etc. Nanolattices derivatives of bio-compatible metal implants augment their performance by allowing improved integration with biological anatomy and processes; the mesh-like structures allow for porosity through the structure allowing for biomaterial exchange as well as a prosthetic cytoskeleton to

promote the growth of endothelial cells. These lightweight nanolattices replicate the structure of myeloid tissue, resulting in a material that is useful for bone implants. This project also pursues the development of structural customizability that would benefit the patient-centered approach in medicine for the design of patient-specific implants for treatment and invasive devices.

5. Budget

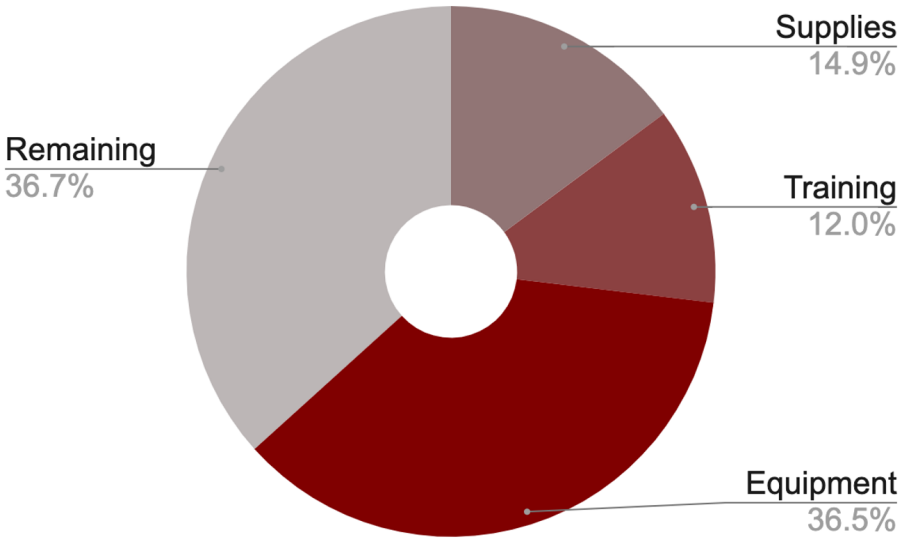

Fig. 4. Breakdown of the total budget used.

The total budget used was $3691, out of a total of $5000.

6. Acknowledgements

Thank you to our SNF mentor Swaroop Kommera and our industry mentor Tony Ricco. Thank you to the course instructor Jonathan Fan, the TA Matti Thurston, and the rest of the E241 teaching staff and mentors along with the SNF and SNSF staff.

7. References

[1] Poltue, Teerapong, Chatchai Karuna, Suppakrit Khrueaduangkham, Saran Seehanam, and Patcharapit Promoppatum. “Design Exploration of 3D-Printed Triply Periodic Minimal Surface Scaffolds for Bone Implants.” International Journal of Mechanical Sciences 211 (December 1, 2021): 106762. https://doi.org/10.1016/j.ijmecsci.2021.106762.

[2] Liu, Y., Wang, H., Ho, J. et al. Structural color three-dimensional printing by shrinking photonic crystals. Nat Commun 10, 4340 (2019). https://doi.org/10.1038/s41467-019-12360-w.
[3] Ye, J., Liu, L., Oakdale, J. et al. Ultra-low-density digitally architected carbon with a strutted tube-in-tube structure. Nat. Mater. 20, 1498–1505 (2021). https://doi.org/10.1038/s41563-021-01125-w.
[4] Vyatskikh, A., Delalande, S., Kudo, A. et al. Additive manufacturing of 3D nano-architected metals. Nat Commun 9, 593 (2018). https://doi.org/10.1038/s41467-018-03071-9.
[5] Ehud Almog, Amit Sharma, Yuanshen Qi, Jonathan Zimmerman, Eugen Rabkin, "Hybrid hierarchical nanolattices with porous platinum coating," Acta Materialia, Volume 225, 2022, 117552, https://doi.org/10.1016/j.actamat.2021.117552.
[6] Wang, Yujia, Xuan Zhang, Zihe Li, Huajian Gao, and Xiaoyan Li. "Achieving the Theoretical Limit of Strength in Shell-Based Carbon Nanolattices." Proceedings of the National Academy of Sciences 119, no. 34 (August 23, 2022): e2119536119. https://doi.org/10.1073/pnas.2119536119.
[7] Bauer, J., Schroer, A., Schwaiger, R. et al. Approaching theoretical strength in glassy carbon nanolattices. Nature Mater 15, 438–443 (2016). https://doi.org/10.1038/nmat4561.
[8] Zhang, Xuan, Andrey Vyatskikh, Huajian Gao, Julia R. Greer, and Xiaoyan Li. "Lightweight, Flaw-Tolerant, and Ultrastrong Nanoarchitected Carbon." Proceedings of the National Academy of Sciences 116, no. 14 (April 2, 2019): 6665–72. https://doi.org/10.1073/pnas.1817309116.
[9] "Nanoscribe User Manual." Nanoscribe GmbH, 30 July 2015.
[10] https://www.osti.gov/servlets/purl/934857
[11] https://aip.scitation.org/doi/full/10.1063/5.0144454